Climate Model Teleconnection Patterns Govern the Niño-3.4 Response to Early Nineteenth-Century Volcanism in Coral-Based Data Assimilation Reconstructions

SARA C. SANCHEZ,[a,c] GREGORY J. HAKIM,[b] AND CASEY P. SAENGER[a]

[a] *Joint Institute for the Study of the Atmosphere and Ocean, University of Washington, Seattle, Washington*
[b] *Department of Atmospheric Sciences, University of Washington, Seattle, Washington*

(Manuscript received 14 July 2020, in final form 3 November 2020)

ABSTRACT: Scientific understanding of low-frequency tropical Pacific variability, especially responses to perturbations in radiative forcing, suffers from short observational records, sparse proxy networks, and bias in model simulations. Here, we combine the strengths of proxies and models through coral-based paleoclimate data assimilation. We combine coral archives (δ^{18}O, Sr/Ca) with the dynamics, spatial teleconnections, and intervariable relationships of the CMIP5/PMIP3 Past1000 experiments using the Last Millennium Reanalysis data assimilation framework. This analysis creates skillful reconstructions of tropical Pacific temperatures over the observational era. However, during the period of intense volcanism in the early nineteenth century, southwestern Pacific corals produce El Niño–Southern Oscillation (ENSO) reconstructions that are of opposite sign from those from eastern Pacific corals and tree ring records. We systematically evaluate the source of this discrepancy using 1) single-proxy experiments, 2) varied proxy system models (PSMs), and 3) diverse covariance patterns from the Past1000 simulations. We find that individual proxy records and coral PSMs do not significantly contribute to the discrepancy. However, following major eruptions, the southwestern Pacific corals locally record more persistent cold anomalies than found in the Past1000 experiments and canonical ENSO teleconnections to the southwest Pacific strongly control the reconstruction response. Furthermore, using covariance patterns independent of ENSO yields reconstructions consistent with coral archives across the Pacific. These results show that model bias can strongly affect how proxy information is processed in paleoclimate data assimilation. As we illustrate here, model bias influences the magnitude and persistence of the response of the tropical Pacific to volcanic eruptions.

KEYWORDS: ENSO; Paleoclimate

1. Introduction

The response of the tropical Pacific to large volcanic eruptions is a longstanding topic of debate. This topic has received considerable attention as volcanic eruptions provide an opportunity to investigate the complex feedbacks and processes driving the ocean and atmospheric responses to perturbations in external radiative forcing. Climate models simulate considerable diversity in the magnitude, persistence, and dynamical responses to volcanic eruptions, even when controlling for differences in eruption size, latitude, and season (Adams et al. 2003; Mann et al. 2005; Emile-Geay et al. 2008; Pausata et al. 2015; Maher et al. 2015; Pausata et al. 2016; Zanchettin et al. 2016; Stevenson et al. 2016; Lehner et al. 2016; Khodri et al. 2017; Stevenson et al. 2018; Zanchettin et al. 2019). Many studies predominantly focus on the short-term response to volcanic eruptions, but additional work has illustrated that volcanic eruptions can elicit a response that persists from decades to centuries (Zanchettin et al. 2012; Pausata et al. 2015; Ding et al. 2014). Successive large eruptions may create a persistent amplified climate response through an accumulation effect (Gupta and Marshall 2018). Statistical and modeling efforts have associated an El Niño–like response to volcanic eruptions (Adams et al. 2003; Mann et al. 2005; Predybaylo et al. 2017; Khodri et al. 2017; Stevenson et al. 2016), but the robustness of this response is dependent on many factors (Emile-Geay et al. 2008; Predybaylo et al. 2017; Ohba et al. 2013; Stevenson et al. 2016) and it may not be detectable relative to the magnitude of unforced variability (Dee et al. 2020b). Furthermore, while many mechanisms have been proposed in models, the dominant dynamics driving the weakened Walker circulation response to volcanic eruptions remain elusive (McGregor and Timmermann 2011; Khodri et al. 2017; Ohba et al. 2013; Stevenson et al. 2016).

This uncertainty stems, in part, from the paucity of instrumental observations of large volcanic eruptions. Over the satellite era, the largest eruption observed is the 1991 Mt. Pinatubo eruption [with a volcanic explosivity index (VEI; Newhall and Self 1982) magnitude of 6], but larger eruptions occurred in the early nineteenth century. Sulfate concentrations in ice cores suggest that the Mystery (1809; VEI 6) and Tambora (1815; VEI 7) eruptions dwarf the 1991 Pinatubo event in magnitude (Gao et al. 2008). Both eruptions are thought to have instigated global repercussions, mostly observed as surface cooling (Stommel and Stommel 1979; Stothers 1984), but the ENSO response remains uncertain. In lieu of direct instrumental observations, simulations of Earth

Supplemental information related to this paper is available at the Journals Online website: https://doi.org/10.1175/JCLI-D-20-0549.s1.

[c] Current affiliation: Department of Atmospheric and Oceanic Sciences, University of Colorado Boulder, Boulder, Colorado.

Corresponding author: Sara C. Sanchez, sara.sanchez@colorado.edu

DOI: 10.1175/JCLI-D-20-0549.1

system models and proxy-based reconstructions both provide a means of investigating the influence of volcanic eruptions on the climate system. However, model-based studies often have known biases poorly constrained initial conditions (Li and Xie 2014; Samanta et al. 2019; Timmreck et al. 2009), while proxies record aspects of the true climate, but with mixed fidelity across an incomplete spatial network.

Fusing information from models and proxies via paleoclimate data assimilation (paleo-DA) has the potential to improve upon reconstructions based on either type of paleoclimate information alone. Paleo-DA is a method of reconstructing full fields of analysis by blending paleoclimate observations within the dynamical constraints of climate models. The Last Millennium Reanalysis, a framework using ensemble Kalman filter data assimilation (DA) methodology, creates paleoclimate reconstructions with small computational cost (Hakim et al. 2016). Using a similar DA methodology, Steiger et al. (2018) show that Niño-3.4 variability can be skillfully reconstructed over the instrumental era (1871–2000) using a global network of tree ring, ice core, coral, and lake core–derived proxies (Emile-Geay et al. 2017) and the CESM Last Millennium Ensemble (Otto-Bliesner et al. 2016) simulations. However, previous paleo-DA efforts have relied heavily on proxy data far removed from the tropical Pacific itself. It is not known if solely using local tropical proxies will yield different results.

Here, we explore the potential of coral-only DA to reconstruct tropical climate variability back to the year 1800 as coral archives are optimally positioned to observe changes in the tropical oceans. Assimilating strictly coral records using the paleo-DA method described below avoids uncertain, nonstationary teleconnections to the midlatitude continents (Coats et al. 2013; Dee et al. 2020a). It has long been suggested that the relationship between midlatitudes and tropical oceans is state dependent, and could be modified under different mean atmospheric conditions or with varied expressions of ENSO (e.g., Cole and Cook 1998; Coats et al. 2013; Batehup et al. 2015). Inaccurate teleconnection or covariance patterns in the climate models could result in unrealistic reconstructions when combined with proxies from the affected regions. Thus, this paleo-DA method provides a test bed to examine the impact of different proxy types, proxies from distinct regions, and the robustness of past climate reconstructions. Differences in reconstructions based on these factors may reveal inaccuracies in the interpretation of proxies or potential errors in the estimation of spatial relationships. As the response of the tropics to the 1809 Mystery and 1815 Tambora eruptions is not known with a high degree of confidence, we use paleo-DA to evaluate the consistency of the tropical response to volcanic eruptions between 1) coral archives and models and 2) coral archives and other types of proxies.

In applying paleo-DA to this problem, we show here that the interpretation of the reconstructed climate from the coral proxy records is strongly dependent on proxy location and the tropical variability of the climate models used in the data assimilation procedure. We proceed with a description of the methods in section 2. Results are presented in section 3, organized around reconstructing the Niño-3.4 index over two intervals: the twentieth century and early nineteenth century. Conclusions are drawn in section 4.

2. Methods

a. Last Millennium Reanalysis methodology

The Last Millennium Reanalysis (LMR; Hakim et al. 2016; Tardif et al. 2019) provides an offline data assimilation framework to integrate networks of paleoclimate proxies within the dynamical constraints of a fixed climate model prior estimate using an ensemble Kalman filter approach (Steiger et al. 2014). With this methodology, we create full field climate reconstructions whereby temporal variability is informed by proxy records and the climate model prior provides dynamical constraints and informs the geospatial and intervariable relationships. We provide an overview of the data assimilation methodology and Kalman update equations, but the complete LMR reconstruction methodology is described elsewhere (Steiger et al. 2014; Hakim et al. 2016; Singh et al. 2018; Tardif et al. 2019). The data assimilation methodology begins with a prior, or estimate of the climate state, $\mathbf{x}_p$. We use the update equation of the Kalman filter (Kalnay 2003) to update this estimate to a new state $\mathbf{x}_a$ that has incorporated information from the proxies $\mathbf{y}$, weighted by the Kalman gain matrix $\mathbf{K}$:

$$\mathbf{x}_a = \mathbf{x}_p + \mathbf{K}(\mathbf{y} - \mathbf{H}\mathbf{x}_p). \tag{1}$$

Matrix $\mathbf{H}$ contains the proxy system model (PSM) information, which models the proxies with relevant physical variables from the prior; for example, many proxies (e.g., tree ring width, coral Sr/Ca, etc.) can be modeled as a function of 2-m air temperature. The difference between the actual proxy value and the estimate $\mathbf{H}\mathbf{x}_p$ is known as the innovation, which contains the new information not already contained in the prior. Following Hakim et al. (2016), we calculate annual anomalies relative to the 1951–80 period and calibrate $\mathbf{H}$ by fitting a linear model to the proxies using GISTEMP (Hansen et al. 2010) surface temperatures during 1850–2015 (see next section for details). The Kalman gain matrix,

$$\mathbf{K} = \mathbf{B}\mathbf{H}^{\mathrm{T}}(\mathbf{H}\mathbf{B}\mathbf{H}^{\mathrm{T}} + \mathbf{R})^{-1}, \tag{2}$$

weights the innovation and spreads it through space and across variables. Here, $\mathbf{B}$ indicates the error covariance matrix for the prior data and $\mathbf{R}$ is the error covariance matrix for the proxies, which we assume to be diagonal. We use the ensemble square root approach to solving (1) and (2) (Whitaker and Hamill 2002), updating the proxy observations annually. We estimate skill over the observational record using two metrics, Pearson's correlation coefficient R and the Nash–Sutcliffe coefficient of efficiency (CE) (Nash and Sutcliffe 1970). When performing paleo-DA with this methodology, the results are potentially sensitive to three key factors: 1) the proxies included in the assimilation (i.e., $\mathbf{y}$), 2) the PSMs used to model the proxies from climate-model data (i.e., $\mathbf{H}$), and 3) climate model prior used to model the proxies and covariance patterns (i.e., $\mathbf{x}_p$, $\mathbf{B}$).

b. Proxies ($\mathbf{y}$)

This paper explores coral-only DA using a network of 125 temperature-sensitive geochemical records that updates previous syntheses (Tierney et al. 2015) and uses all available coral

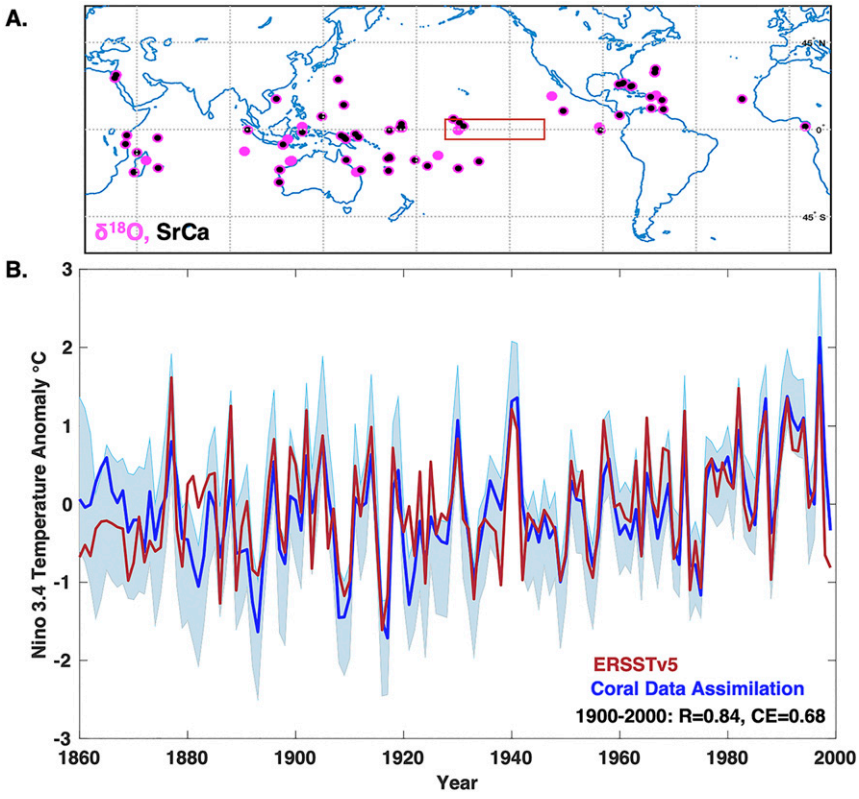

FIG. 1. (a) Locations of coral records used in this analysis (δ^{18}O in pink, Sr/Ca in black; full report can be found in Table S1). The Niño-3.4 region is outlined in red. (b) The Niño-3.4 index relative to the 1951–80 mean in NOAA ERSSTv5 (red) and in the LMR-CCSM4 coral reconstruction (blue). Light blue shading represents the reconstruction 95% confidence intervals.

records from the NOAA paleoclimate archive spanning more than 40 years as of March 2019 (Fig. 1a; see also Table S1 in the online supplemental material). Of these, 40 records are based on the ratio of strontium to calcium (Sr/Ca), and 85 measure the coral's oxygen isotope composition (δ^{18}O). This network adds 25 publicly available records from the NCEI NOAA Paleoclimate archive to the PAGES 2k database. The full PAGES2k network (Emile-Geay et al. 2017), which includes tree rings, ice cores, and corals from a variety of regions and sources is used as a reference reconstruction, but the main experiments described here depend solely on coral records. Proxy availability decreases with time such that the coral-only network consists of 125 records over the twentieth century, but diminishes to 39 records by the year 1830.

c. *Proxy system models (***H***)*

Proxy system models (PSMs) refer to a model of the physical, chemical, and biological processes that allow environmental information to be derived from a geochemical archive (Evans et al. 2013; Thompson et al. 2011; Dee et al. 2015). To constrain the true variability of the climate system, it is necessary to account for any processes that may influence the geochemical signals within the proxy archives independent of the environmental variable of interest (e.g., temperature). In corals, both Sr/Ca and δ^{18}O are highly correlated with local temperature. Sr/Ca is typically interpreted to reflect temperature alone (Beck et al. 1992), and δ^{18}O to reflect a combination of temperature and the δ^{18}O of seawater ($\delta^{18}O_{sw}$), assuming biological vital effects are constant (Epstein et al. 1953; Weber and Woodhead 1972; Thompson et al. 2011; Stevenson et al. 2015; Lawman et al. 2020). In turn, $\delta^{18}O_{sw}$ is often highly correlated with sea surface salinity as both are controlled by the processes of precipitation and evaporation (Cole and Fairbanks 1990; Fairbanks et al. 1997; Conroy et al. 2014). In the LMR approach, both coral Sr/Ca and δ^{18}O anomalies are modeled as a univariate, linear function of temperature with an error term ε (Hakim et al. 2016):

$$\text{Coral}\,\Delta\delta^{18}\text{O} = a_1\Delta\text{SST} + \varepsilon, \tag{3}$$

$$\text{Coral}\,\Delta\text{Sr/Ca} = b_1\Delta\text{SST} + \varepsilon. \tag{4}$$

While this traditional model is well equipped to handle variations in coral geochemistry due to temperature, we note that this simplified PSM does not properly account for additional variability in the coral δ^{18}O due to variations in $\delta^{18}O_{sw}$ associated with precipitation, evaporation, or ocean circulation. To properly represent this additional complexity, decades-long high-fidelity observational products of $\delta^{18}O_{sw}$ or sea surface

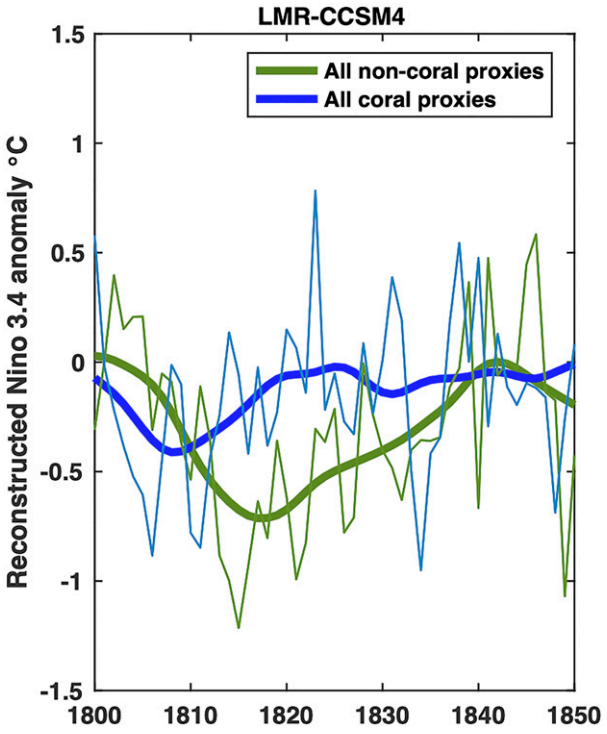

FIG. 2. Reconstructions of Niño-3.4 temperature by proxy type with NCAR-CCSM4 prior, anomaly relative to the 1951–80 mean. The non-coral experiment (predominantly tree ring and ice core measurements) is in green and the coral-only experiment in blue. There is a sustained offset between the reconstructions from about 1809 to 1830. The records spanning 1809–30 are listed in Table 1, and shown in Fig. 4.

salinity variability that overlap with coral records are needed to calibrate the appropriate coefficients in the PSMs.

d. Prior ($\mathbf{x}_p$)

We predominantly use the NCAR CCSM4 Past1000 simulation as a prior for our experiments (Otto-Bliesner et al. 2014), although other CMIP5/PMIP3 models are ultimately considered (see section 3c below). The CCSM4 Past1000 simulations has the same standard 1° resolution as CCSM4 and simulates fairly realistic ENSO dynamics and teleconnection patterns, but still features several biases common to climate models, such as exaggerated ENSO variance and a cold tongue bias (Deser et al. 2012). This experiment simulates the years 850–1850, with prescribed last millennium greenhouse gas, volcanic, solar, and land use change forcings (Schmidt et al. 2011). This simulation samples a wide range of realistic climate states that provides an opportunity to test the sensitivity of the reconstructions to this choice.

3. Results and discussion

We first evaluate the skill of the reconstructed SST fields by examining the relationship between our coral reconstructions with calculations of the Niño-3.4 index (SST anomaly averaged over 5°N–5°S, 170°–120°W) from observational reanalysis during the twentieth century [including NOAA ERSSTv5 (Huang et al. 2017), COBE SST2 (Hirahara et al. 2014), HadISST (Rayner et al. 2003), SODA2.2.4 (Giese and Ray 2011), and Kaplan (Kaplan et al. 1997)]. Coral-only DA is skillful (Fig. 1b, Tables S2–S6) and outperforms the all-proxy reconstructions of Niño-3.4. For example, Niño-3.4 observations from NOAA ERSSTv5 over the years 1900–2000 have $R = 0.84$ and CE = 0.68 with reconstructions from coral-only DA, while all-proxy reconstructions have an $R = 0.77$, CE = 0.59. This improvement in skill potentially occurs because coral-only DA only considers proxy archives from the tropical oceans (Fig. 1a), as opposed to teleconnected regions. Additional comparisons of coral-only DA to all-proxy DA using other priors and reanalysis products exhibit similar results (Tables S2–S6).

While this method of reconstruction is skillful and in agreement with other proxy archives over the observational era, extending the Niño-3.4 reconstruction to the year 1800 generates unexpected results during the period of intense volcanism from 1809 to 1830. The coral-only DA reconstruction over the early nineteenth century suggests decades-long periods of relatively warm equatorial Pacific temperatures (relative to the 1951–80 mean). In comparison, paleo-DA reconstructions using all data except corals show anomalously cool conditions from 1809 to 1830 that are ~0.5°C cooler than coral-only reconstructions (Fig. 2); a substantial offset given the close agreement of the reconstructions over the rest of the nineteenth and twentieth centuries (not shown). This result is further surprising as this period occurs toward the end of the Little Ice Age, known for persistent, relatively cool conditions in the Northern Hemisphere (e.g., Crowley et al. 2014; Brönnimann et al. 2019), possibly associated with increased volcanism. This interproxy discrepancy, or the difference in mean Niño-3.4 anomaly over the 1809–30 period between the coral-only and non-coral reconstructions, has important implications for how the Niño-3.4 region responds to intense radiative forcing, making it crucial to determine if the coral-only reconstruction is more realistic or an artifact of the paleo-DA methodology.

We examine the source of this discrepancy and evaluate plausible causes by addressing three questions: 1) Do the assumptions in the coral PSMs strongly affect the results? 2) Does the number or spatiotemporal distribution of proxy data introduce a bias in the results? 3) How sensitive are the reconstructions to the covariance patterns of individual models? We examine each question sequentially.

a. Do the assumptions in the coral PSMs strongly affect the results?

It is well established that coral $\delta^{18}O$ is sensitive to changes in $\delta^{18}O_{sw}$, and interpreting coral $\delta^{18}O$ as a univariate function of temperature in our PSM could contribute to the discrepancy in Niño-3.4 reconstructions (Fig. 2). To evaluate this possibility, we employ a bivariate PSM that accounts for $\delta^{18}O_{sw}$ variability using its relationship with sea surface salinity [SSS; Eq. (5)] instead of the simplified univariate PSM [Eq. (3)]. The bivariate coral $\delta^{18}O$ PSM (Thompson et al. 2011) is given by

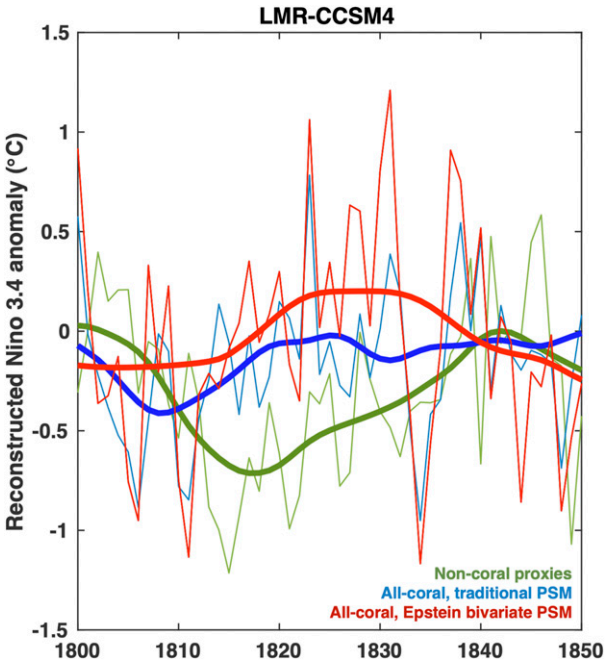

FIG. 3. As in Fig. 2, but with the addition of a reconstruction assimilating corals with a bivariate PSM. The incorporation of a more realistic PSM does not correct the sustained interproxy discrepancy from 1809 to 1830.

$$\text{Coral}\,\Delta\delta^{18}\text{O} = a_1\Delta\text{SST} + a_2\Delta\text{SSS} + \varepsilon, \tag{5}$$

where $a_1 = -0.22‰$ (Epstein et al. 1953; Lough et al. 2004; Thompson et al. 2011; Kim and O'Neil 1997; O'Neil et al. 1969) and a_2 is solved for using a best-fit linear regression between the temperature residual (GISTEMP; Hansen et al. 2010) and local salinity (ORA20C ocean reanalysis SSS; de Boisséson et al. 2018).

This modification provides skillful reconstructions of the Niño-3.4 index over the twentieth century ($R = 0.87$, CE = 0.66, compared to the linear PSM reconstruction results of $R = 0.84$ and CE = 0.68), but leads to even warmer Niño-3.4 reconstructions over the 1809–30 interval (Fig. 3). We do not interpret this result as evidence that the bivariate PSM is less accurate than the linear PSM. The greater discrepancies using a bivariate PSM may be explained, in part, by how SSS products are generated. The paucity of SSS observations poses a challenge for coral–SSS calibration. The ARGO program (ARGO; Roemmich and Gilson 2009) has transformed observational networks of salinity, but only extends globally to 2004. Many of the longer salinity reanalysis products are driven by assimilating sea surface temperature, temperature, and salinity profiles, and occasionally sea surface altimetry (Shi et al. 2017). Thus, it is possible that the interproxy discrepancy increases when adopting the bivariate PSM because the calibration process is compromised by the lack of actual observations of SSS.

Furthermore, although there is precedent for using salinity as a proxy for $\delta^{18}O_{sw}$ in PSMs (e.g., Cole and Fairbanks 1990; Fairbanks et al. 1997; Thompson et al. 2011; Dee et al. 2015; Russon et al. 2013), salinity is not an exact substitute for $\delta^{18}O_{sw}$. Salinity and $\delta^{18}O_{sw}$ are highly correlated spatially in the modern ocean (LeGrande and Schmidt 2006) because they are both influenced by precipitation, evaporation, and oceanic circulation. However, it is difficult to confirm that these spatial relationships are valid temporally, especially over many decades (Stevenson et al. 2018). Recent modeling efforts have included isotope enabled experiments, so it is possible that future coral DA efforts could assimilate $\delta^{18}O_{sw}$ directly. Confidence in assimilating $\delta^{18}O_{sw}$ could be improved with long-term station monitoring of oxygen isotopes in seawater from geographically diverse regions and more isotope-enabled general circulation models.

b. Does the number or spatiotemporal distribution of proxy data introduce a bias in the results?

While there are 125 total coral records, only 39 (12 Sr/Ca; 27 $\delta^{18}O$) provide annually resolved data over the years 1809–30 (Table 1). When using the LMR framework to reconstruct each proxy's local temperature (i.e., single-proxy reconstructions without influence from other proxies), the majority of these 39 coral records yield evidence for cooler temperatures (relative to the 1951–80 mean) at their own location over the 1809–30 interval using CCSM4 as a prior (Fig. 4). These local reconstructions suggest that the persistent, warmer, Niño-3.4 reconstruction (Fig. 2) is related to how information from individual coral records is spread from the record location onto the Niño-3.4 region by the climate model prior. We conduct additional experiments by dividing corals into geographical subsets to better understand how information from each region affects the reconstructed Niño-3.4.

To evaluate how coral records from specific geographic regions influence Niño-3.4 reconstructions, we divide the proxies into regional groups (i.e., Atlantic, Indian, western Pacific, and eastern Pacific). Reconstructions with only coral data (coral-only) and all PAGES2K data except corals (non-coral) are used for comparison. Of these geographically divided subsamples, only western Pacific corals produce a warm Niño-3.4 anomaly (Fig. 5), suggesting that this region is responsible for the relatively warm Niño-3.4 reconstruction when using all coral data (Fig. 2). This warm anomaly is particularly prevalent when only $\delta^{18}O$ records are considered (Fig. 5). Of the 39 corals spanning 1809–30, 15 corals (nearly 40% of available coral records) are from the western Pacific, illustrating that the interproxy discrepancy is not the result of a small number of outlier records. Additionally, the western Pacific coral records, mostly located in the SPCZ region (12 out of 15), are generally in agreement that cooler conditions persisted locally over the 1809–30 interval, suggesting that the covariability between the SPCZ region and Niño-3.4 region is responsible.

c. How sensitive are the reconstructions to the covariance patterns of individual models?

We explore the role of the climate model prior as the source of the interproxy discrepancy in Niño-3.4 reconstructions. We expand our choice of priors to include the 10 CMIP5/PMIP3

TABLE 1. Identification of coral proxies included in this study to assess variability over the 1800–30 period. Each proxy is labeled with a location classification and further relevant information is included.

	Location ID	Record	Variable	Lat (°)	Lon (°)	Years		Author	DOI
1	Pacific, West-SPCZ	Ta'u American Samoa	$\delta^{18}O$	−14.3	190.5	1520	2011	Tangri et al. (2018)	10.1029/2017PA003310
2	Pacific, West-SPCZ	New Caledonia	$\delta^{18}O$	−22.5	166.5	1657	1992	Quinn et al. (1998)	10.1029/98PA00401
3	Pacific, West-SPCZ	Savu Savu Bay, Fiji	$\delta^{18}O$	−16.8	179.2	1776	2001	Bagnato et al. (2005)	10.1029/2004GC000879
4	Pacific, West-SPCZ	Rarotonga, Cook Islands	$\delta^{18}O$	−21.2	200.2	1727	1996	Linsley et al. (2006)	10.1029/2005GC001115
5	Pacific, West-SPCZ	Fiji-AB	$\delta^{18}O$	−16.8	179.2	1618	2001	Linsley et al. (2006)	10.1029/2005GC001115
6	Pacific, West-SPCZ	Fiji-1F	$\delta^{18}O$	−16.8	179.2	1782	1996	Linsley et al. (2006)	10.1029/2005GC001115
7	Pacific, West-SPCZ	Vanuatu	$\delta^{18}O$	−15.0	167.0	1807	1979	Quinn et al. (1996)	10.1029/96GL03169
8	Pacific, West-SPCZ	Abraham Reef, Australia	$\delta^{18}O$	−22.1	153.0	1638	1983	Druffel and Griffin (1999)	10.1029/1999JC900212
9	Pacific, West-SPCZ	Fiji-1F	Sr/Ca	−16.8	179.2	1782	1996	Linsley et al. (2006)	10.1029/2005GC001115
10	Pacific, West-SPCZ	Hafera Island, Tonga	Sr/Ca	−19.9	185.3	1791	2003	Wu et al. (2013)	10.1029/2005GC004293
11	Pacific, West-SPCZ	Amedee Island, New Caledonia	Sr/Ca	−22.5	166.5	1649	1999	DeLong et al. (2012)	10.1038/nclimate1583
12	Pacific, West-SPCZ	Rarotonga, Cook Islands	Sr/Ca	−21.2	200.2	1618	1996	Linsley et al. (2006)	10.1029/2005GC001115
13	Pacific, West	Double Reef, Guam	$\delta^{18}O$	13.6	144.8	1790	1999	Asami et al. (2005)	10.1029/2004JC002555
14	Pacific, West	Ulong Channel, Palau	$\delta^{18}O$	7.3	134.3	1793	2007	Osborne et al. (2014)	10.1007/s00338-014-1146-1
15	Pacific, West	New Ireland, Papua	Sr/Ca	−2.5	150.5	1823	1996	Alibert and Kinsley (2008)	10.1029/2007JC004263
16	Pacific, East	Clarion Island, Revillagigedos, Mexico	$\delta^{18}O$	18.4	245.3	1819	1997	Sanchez et al. (2016)	10.1002/2016GL069037
17	Pacific, East	Urvina Bay, Galapagos	$\delta^{18}O$	−0.4	268.8	1607	1981	Dunbar et al. (1994)	10.1029/93PA03501
18	Pacific, East	Secas Island, Panama	$\delta^{18}O$	8.0	278.0	1708	1983	Linsley et al. (1994)	10.1029/94JC00360
19	Atlantic	Biscayne Bay, Florida, United States	$\delta^{18}O$	25.4	279.8	1751	1986	Swart et al. (1996a)	10.2307/3515246
20	Atlantic	Florida Bay, Florida, United States	$\delta^{18}O$	24.9	279.3	1824	1985	Swart et al. (1996b)	10.1016/00.31-0182(95)00078-X
21	Atlantic	North east Breakers, Bermuda	$\delta^{18}O$	32.5	295.3	1825	1982	Kuhnert et al. (2005)	10.1029/2004GC000786
22	Atlantic	Atlantic	$\delta^{18}O$	17.9	293.0	1751	2004	Kilbourne et al. (2008)	10.1029/2008PA001598
23	Atlantic	Bermuda South Shore	$\delta^{18}O$	30.6	295.0	1782	1998	Goodkin et al. (2008)	10.1038/ngeo352
24	Atlantic	Turrumote Reef, Puerto Rico	$\delta^{18}O$	17.9	293.0	1751	2004	Kilbourne et al. (2008)	10.1029/2008PA001598
25	Atlantic	Bermuda South Shore	Sr/Ca	30.6	295.0	1781	1998	Goodkin et al. (2008)	10.1038/ngeo352
26	Atlantic	Dry Tortugas	Sr/Ca	24.6	277.7	1734	2007	DeLong et al. (2014)	10.1002/2013PA002524
27	Indian	Aqaba, Jordan	$\delta^{18}O$	29.4	35.0	1788	1992	Heiss et al. (1999)	10.1007/BF03042826
28	Indian	Ifaty	$\delta^{18}O$	−23.2	43.6	1660	1994	Zinke et al. (2004)	10.1016/j.epsl.2004.09.028
29	Indian	Lombok, Indonesia	$\delta^{18}O$	−8.2	115.6	1782	1989	Charles et al. (2003)	10.1016/S0025-3227(03)00217-2
30	Indian	Darwin Long (DL), Cocos (Keeling) Islands	$\delta^{18}O$	−12.1	96.9	1808	2009	Hennekam et al. (2018)	10.1002/2017PA003181
31	Indian	Nusa Penida, Lombok Strait, Indonesia	$\delta^{18}O$	−8.7	115.5	1824	2015	Murty et al. (2018)	10.1029/2018PA003387
32	Indian	Houtman Abrohos	$\delta^{18}O$	−28.5	113.8	1795	1993	Kuhnert et al. (1999)	10.1007/s003380050147
33	Indian	Malindi	$\delta^{18}O$	−3.2	40.1	1801	1994	Cole et al. (2000)	10.1126/science.287.5453.617
34	Indian	Darwin Long (DL), Cocos (Keeling) Islands	Sr/Ca	−12.1	96.9	1808	2009	Hennekam et al. (2018)	10.1002/2017PA003181
35	Indian	Ifaty Reef, SW Madagascar, 04mada01a	Sr/Ca	−23.2	43.6	1659	1994	Zinke et al. (2004)	10.1016/j.epsl.2004.09.028
36	Indian	Imperieuse Reef, Rowley Shore, Australia IMP03A	Sr/Ca	−17.5	119.0	1806	2009	Zinke et al. (2015)	10.1038/ncomms9562
37	Indian	Imperieuse Reef, Rowley Shore, Australia IMP05A	Sr/Ca	−17.5	119.0	1798	2009	Zinke et al. (2015)	10.1038/ncomms9562
38	Indian	Houtman Abrolhos	Sr/Ca	−28.5	113.8	1798	2010	Zinke et al. (2014)	10.1038/ncomms4607
39	Indian- Red Sea	Red Sea	$\delta^{18}O$	27.9	34.3	1751	1995	Felis et al. (2000)	10.1029/199PA000477

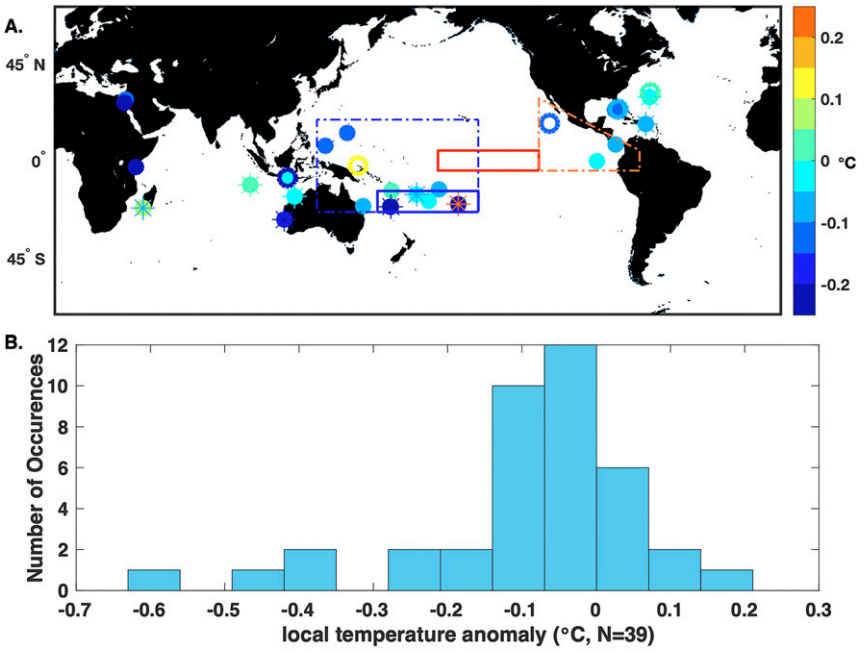

FIG. 4. (a) Coral single-site reconstructions of mean local temperature anomaly over 1809–30 (corals do not inform the reconstruction anywhere but their location). Records that do not extend the full period are unfilled. Multiple coral records in the same grid box are denoted with an asterisk (*). The Niño-3.4 region is outlined in bold red, the SPCZ region outlined in bold blue, the western Pacific region outlined in dashed blue, and the eastern Pacific region outlined in dashed orange. (b) Histogram of local anomalies from (a). Most available coral records suggest cold anomalies over this interval.

Past1000 experiments (BCC-CSM1-1, NCAR-CCSM4, CSIRO-Mk3L-1-2, FGOALS-GL, GISS-E2-R, HadCM3, IPSL-CM5A-LR, MIROC-ESM, MPI-ESM-P, MRI-CGCM3) and 5 of the NCAR-CESM Last Millennium Ensemble (LME) simulations for our experiments (Table 2). The CMIP5/PMIP3 and the NCAR-CESM LME priors provide a range of physically realistic possible background states. For example, ENSO features substantial differences in magnitude of variability and diversity of simulated teleconnection patterns between the experiments (Bellenger et al. 2014). Table 2 provides further details of the relevant characteristics of the PMIP3/CMIP5 Past1000 model simulations used here. The wide range of climate model simulations provides an opportunity to test the sensitivity of the reconstructions to this choice. To assess whether the dynamics of CCSM4 are responsible for the early-nineteenth-century interproxy discrepancy, we replicate the experiment of reconstructing the Niño-3.4 index using the non-coral, coral-only, and regional coral proxies over the years 1809–30 for all model priors (Fig. 6).

We find a wide range in the magnitude of interproxy discrepancy among the priors, including both positive and negative anomalies (Fig. 6). Seventy-five percent (12/16) of all-coral experiments show a warmer 1809–30 temperature anomaly than their complementary non-coral reconstruction, indicating that the interproxy discrepancy observed using CCSM4 is not unique to that single model (Fig. 6, Table S7). The sign and magnitude of the discrepancies are not directly related to the skill of the prior over ''normal'' conditions as all priors reliably reconstruct the twentieth century Niño-3.4 (Tables S2–S6). Repeating the geographically localized proxy reconstructions (i.e., Fig. 4) suggests that the western Pacific region is again the main source of the warm anomaly in all-coral reconstructions for many of the priors, particularly LME simulations (Fig. 6). A minority of priors (e.g., IPSL, MIROC, GISS, and MPI) yield all-coral Niño-3.4 reconstructions that are cooler than the non-coral reconstructions, and show less anomalous reconstructed behavior in the west Pacific (Fig. 6). As described below, this result can largely be attributed to modeled covariance between the Niño-3.4 and SPCZ regions.

There is a large range in correlation coefficients between the sea surface temperature of the SPCZ and Niño-3.4 regions, ranging from +0.61 in the MIROC model to −0.68 in the CESM LME (Table 2, Fig. 7). For comparison, the correlation between these regions in Twentieth Century Reanalysis (20CR; Compo et al. 2011) is −0.36. This highlights the considerable and well-documented model biases in the southwest Pacific, occasionally referred to as the ''double ITCZ problem'' (e.g., Brown et al. 2011; Irving et al. 2011; Lin 2007). Using 20CR as a prior in the data assimilation, we also find a persistent, warm Niño-3.4 anomaly over the 1809–30 period (Figs. 6 and 7), further illustrating that the discrepancy is not a reflection of the quality of the prior. Taken together, the results for all priors reveal a clear, linear relationship between

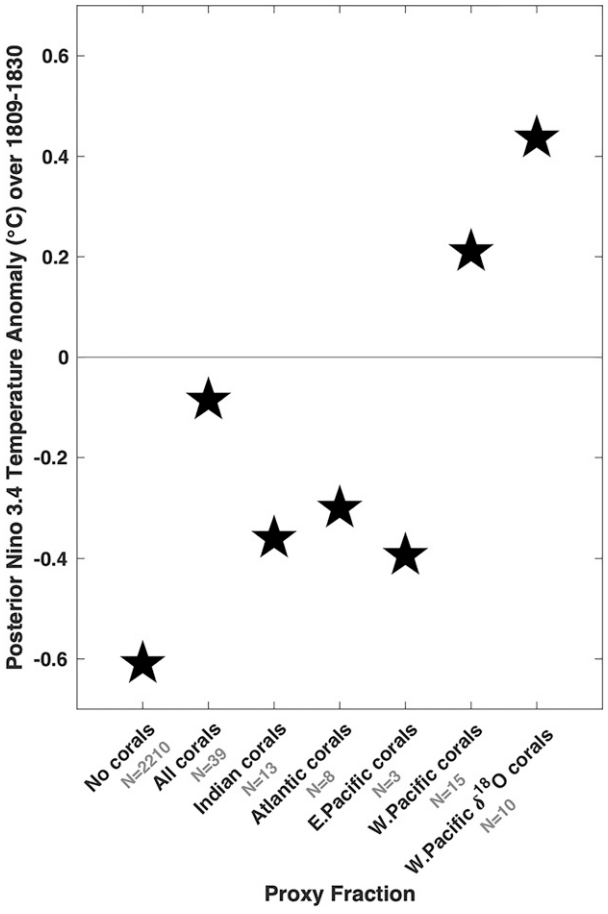

FIG. 5. Reconstructed mean Niño-3.4 temperatures averaged over 1809–30 from reconstructions using the CCSM4 prior assimilating non-coral proxies, coral-only, and corals from subregions. The *N* refers to the number of coral records in each region. Coral-based reconstructions generate a much wider spread of estimated Niño-3.4 behavior, especially corals from the western Pacific, suggesting this region may be responsible for discrepancies in Fig. 2.

reconstructed coral-only Niño-3.4 temperature anomaly and the prior's correlation between the SPCZ and Niño-3.4 regions (Fig. 7). We consider two hypotheses for this linear relationship: 1) it is the result of state-dependent response to volcanic eruptions and 2) ENSO teleconnections are exclusively responsible for the interproxy discrepancy, even during periods of substantial volcanic activity.

If the first hypothesis was correct, we would expect the interproxy discrepancy to be reduced by sampling from a range of volcanic eruptions with different background states. The CESM-LME is an ensemble that contains 18 volcanically forced last millennium simulations, and provides an opportunity to conditionally sample a variety of volcanic initial conditions. Specifically, we create a prior by sampling only the volcanically active 1800–50 period in the LME, yielding a 900-member ensemble influenced by 36 large volcanic eruptions (18 unique simulations of the 1809 Mystery Eruption, and 18 simulations of the 1815 Tambora eruption, greater detail of the prior can be found in Table 3). This ''super volcano'' experiment marginally decreases the interproxy discrepancy, illustrated by the *y* axis, when compared to the CESM-LME experiments (Fig. 7, labeled, filled circle). This suggests that the appropriate conditions at the time of the volcanic eruption have an influence on the reconstruction, at least as this response is simulated by climate models, but ultimately does not support our first hypothesis and cannot explain the large interproxy discrepancy. This result also introduces the possibility that the covariance relationships of the volcanic states are still vulnerable to the biases in the climate model mean state. Even with appropriate volcanic forcing, the persistent biases in the tropical mean state modify covariance patterns and could influence the interproxy discrepancy.

We consider our second hypothesis by breaking traditional ENSO teleconnections in two ways: 1) using a slab ocean experiment from the CESM Large Ensemble (CESM-LE; Kay et al. 2015) as a prior, which cannot support a ''true'' ENSO without ocean dynamics, and 2) using a series of ''El Nada'' (i.e., neither El Niño nor La Niña) priors from the CESM-LME experiments where the magnitudes of anomalies in the Niño-3.4 region are screened below thresholds of 0.35°, 0.25°, 0.15°, and 0.05°C. The unforced slab ocean simulation from CESM-LE employs a CESM1-CAM5 atmosphere (Hurrell et al. 2013), as does CESM-LME; however, the CESM-LME uses a coarser-resolution atmosphere and land grid. As expected, the slab ocean model displays a much weaker correlation between the Niño-3.4 and SPCZ region and the reconstruction based on the slab-ocean model shows a reduced interproxy discrepancy. Moreover, the El Nada experiments also show a similar trend with reduced Niño-3.4 variance corresponding to a weaker correlation between Niño-3.4 and SPCZ regions, and a smaller interproxy discrepancy (Table 3, Fig. 7). This supports our second hypothesis, and indicates that the interproxy discrepancy observed in Fig. 2 can largely be attributed to model covariance patterns. Consistent with this, we find a positive linear relationship between the magnitude of Niño-3.4 variability in the fixed model prior and the magnitude of the interproxy discrepancy (Table 3, Fig. 8).

d. Volcanic and ENSO-like climate variability

This work emphasizes the difficulties of disentangling the climate response to volcanic eruptions from ENSO. It is important to differentiate ENSO from the multiyear equatorial warming described extensively here. We consider an El Niño (or La Niña) event to be a warm (cold) deviation from the mean state that persists for a single year, which is distinctly different from many of the coral-only reconstructions, which indicate a highly persistent, decades-long warm state in the equatorial Pacific. Authors of individual coral archives from the SPCZ region describe cooler, drier conditions over this period, but do not suggest that this is evidence for a prolonged warm state in the equatorial Pacific (e.g., Linsley et al. 2006). In fact, high-resolution $\delta^{18}O$ and radiocarbon records from the eastern equatorial Pacific (not included in this reconstruction due to the lack of modern coral measurements upon which to

TABLE 2. Priors used in this study and several metrics of tropical climate variability: the standard deviation of the Niño-3.4 region (5°S–5°N, 170°–120°W), standard deviation of the SPCZ region (15°–25°S, 160°–210°E), and the Pearson's correlation coefficient between the Niño-3.4 and SPCZ regions in the prior.

Prior model/reanalysis	Abbreviation	Standard deviation of Niño-3.4 (°C)	Standard deviation of SPCZ region (°C)	Pearson's correlation coefficient (R) of Niño-3.4 and SPCZ
CSIRO-Mk3L-1–2 (Australia's Commonwealth Scientific and Industrial Research Organization)	CSIRO	0.42	0.21	−0.35
NCAR-CCSM4 (National Center for Atmospheric Research)	CCSM4	0.67	0.26	−0.29
BCC-CSMI-1 (Beijing Climate Center)	BCC	0.47	0.15	−0.22
FGOALS-GL (Flexible Global Ocean–Atmosphere–Land–Sea ice)	FGOALS	0.86	0.15	0.01
GISS-E2-R r1i1p121 (Goddard Institute for Space Studies)	GISS	0.39	0.22	0.09
HadCM3 (Hadley Centre Coupled Model)	HadCM3	0.59	0.26	−0.19
IPSL-CM5-LR (Institute Pierre Simson Laplace)	IPSL	0.50	0.20	0.19
MIROC-ESM (Model for Interdisciplinary Research on Climate)	MIROC	0.40	0.25	0.61
MPI-ESM-P (Max Planck Institute)	MPI	0.60	0.23	−0.02
MRI-CGCM3 (Meteorological Research Institute)	MRI	0.44	0.17	−0.20
NCAR-CESM-LME-A1 (National Center for Atmospheric Research)	MEA1	0.99	0.27	−0.68
NCAR-CESM-LME-A2 (National Center for Atmospheric Research)	MEA2	0.96	0.27	−0.68
NCAR-CESM-LME-A3 (National Center for Atmospheric Research)	MEA3	0.94	0.27	−0.68
NCAR-CESM-LME-A4 (National Center for Atmospheric Research)	MEA4	0.97	0.27	−0.68
NCAR-CESM-LME-A5 (National Center for Atmospheric Research)	MEA5	0.94	0.26	−0.68
NOAA Twentieth Century Reanalysis	20CR	0.39	0.29	−0.36

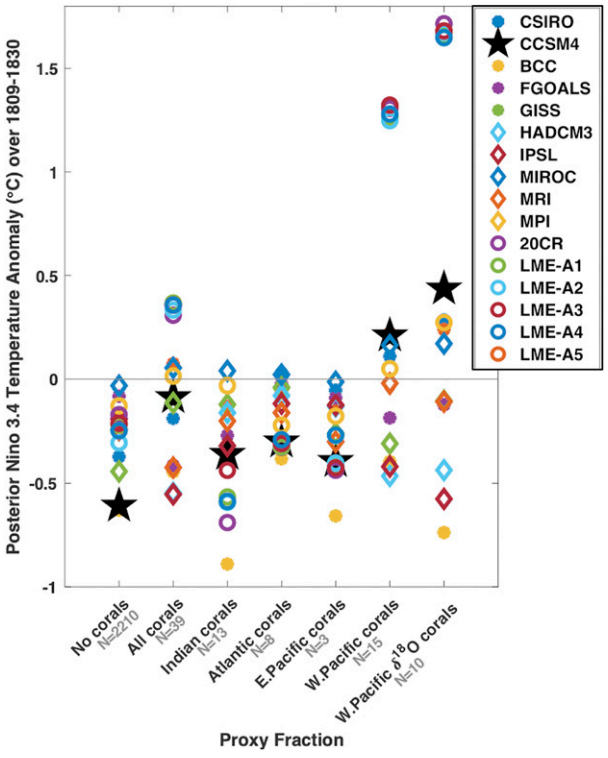

FIG. 6. As in Fig. 4, but considering multiple climate model priors. The 1809–30 average for each prior is plotted with a single data point. The results from CCSM4 in Fig. 4 are illustrated with black stars. Coral-based reconstructions yield a much wider spread of estimated Niño-3.4 behavior, especially corals from the western Pacific.

calibrate PSMs) identified frequent La Niña events during the early nineteenth century (Druffel et al. 2015). The results here indicate that prolonged SPCZ cooling are accompanied by individual years of warm, neutral, and even cold conditions in the equatorial Pacific, but the model covariance patterns determine the range of mean conditions of the reconstructions in the decades following these eruptions. Further experiments assimilating corals from all regions except the western Pacific with each of the 10 Past1000/Last Millennium priors provide evidence for cool conditions across the equatorial Pacific during the eruption year and two years following (1809–11, 1815–17) for both the Mystery and Tambora eruptions in the multireconstruction mean (Fig. S1). These experiments eliminate bias from teleconnection patterns between the Niño-3.4 and western Pacific, but they reconstruct lower magnitude cool anomalies in the South Pacific convergence zone relative to the all-coral reconstructions. When considering the gradient of temperature anomalies across the equatorial Pacific, a high diversity of responses ranging from El Niño–like to La Niña–like arise, dependent on the model used as a prior in the experiment (Fig. S2–S7). However, we note that despite the diversity in coral-DA reconstructions, there are still stark differences between the multimodel mean and multireconstruction mean. For example, in the year 1816, all coral-DA reconstructions with each of the Past1000/Last Millennium priors indicate cool anomalies across the equatorial Pacific (Figs. S6a–j; see also the multi-reconstruction mean in Fig. S6k), but the multimodel mean (not informed by proxies) indicates modest equatorial warming (Fig. S6l).

An interesting outcome of modifying the volcanically forced prior is the finding that, in some models, such as the CESM-LME, years when Niño-3.4 and SPCZ have simultaneous cold anomalies (greater than one standard deviation) in the annual average are exceedingly rare. Such simultaneous cold anomalies only occur 47 times in the combined suite of 18 000 years of volcanically forced CESM LME simulations, or 0.26% of the time. Within the other 10 volcanically forced PMIP3/CMIP5 Past1000 priors used in this study, the mean rate of occurrence of simultaneous cold anomalies is 2.9% of the time (Table S7). While twentieth-century observations have not been forced with large volcanic eruptions, we find two simultaneous Niño-3.4-SPCZ cold anomalies in ERSSTv5 reanalysis in the years 1886 and 1909. These years are not known for large volcanic eruptions, but are recognized as years featuring a substantial La Niña event. We also note that instrumental observations of the SPCZ region temperature variability have more variance than many of the CMIP5/PMIP3 Past1000 and CESM-LME models (Table 2). Still, when the twentieth-century reanalysis is used as the prior, we find the interproxy discrepancy biased for warm equatorial conditions, indicating that this stationary covariance pattern is particularly problematic when simulating the post-eruption response.

e. Volcanic and southwestern Pacific climate variability

Comparing SPCZ region behavior in the Past1000 climate simulations to the coral-based LMR reconstructions (Figs. 9a–c) reveals that while the models tend to simulate diverse, short-lived, large-magnitude responses, the LMR reconstructions consistently indicate persistent cooler, drier conditions in the SPCZ region during the early nineteenth century, with surprising coherence, regardless of the prior used (Figs. 9b,c). Moreover, the magnitude of the cold anomalies in the reconstruction appears to be controlled by the SPCZ variance in the prior (Figs. 9d,e). Despite the inherent uncertainties in model simulations of this region, this result indicates that the proxies are driving this strong SPCZ regional response. We note a distinct difference in the magnitude and persistence of the reconstructed anomalies when reconstructing using combined Sr/Ca and $\delta^{18}O$ proxies ($N = 15$), or just $\delta^{18}O$ proxies ($N = 10$). Reconstructions using solely $\delta^{18}O$ records from the western Pacific yield a more persistent response of lower amplitude, likely due to the multivariate nature of the $\delta^{18}O$ signal. In the western Pacific, $\delta^{18}O_{sw}$ variability has been shown to have higher relative influence on coral $\delta^{18}O$ in isotope-enabled climate models (Russon et al. 2013) and observations (Conroy et al. 2017) because of large hydrologic variability and relatively stable warm temperatures. We do not attempt to dissect the multivariate SPCZ signal, but acknowledge its significance and emphasize that refining the coral $\delta^{18}O$ bivariate PSM could be a useful direction for future work.

It is fairly straightforward to compare the volcanic response in climate models with paleoclimate data assimilation reconstructions in regions of high proxy density or when

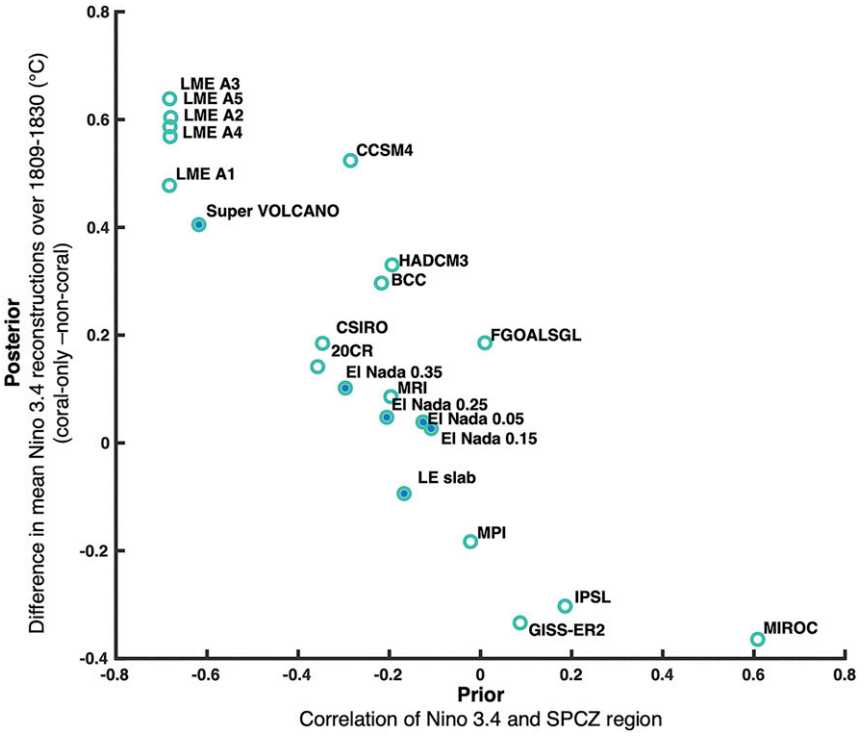

FIG. 7. Scatterplot of the relationship between the correlation coefficient of the Niño-3.4 and SPCZ region in the prior and the magnitude of the reconstructed interproxy discrepancy. Priors are sourced from the PMIP3/CMIP5 priors (unfilled circles) and super prior (filled circles) experiments.

incorporating priors that feature accurate covariance patterns. However, in regions with sparse observations and inconsistent or inaccurate covariance patterns, it is difficult to evaluate the true climate response. The coral paleo-DA approach provides clear evidence for persistent cooler, drier conditions in the SPCZ region after the eruptions of the early nineteenth century. However, the diversity of covariance patterns in the Past1000/Last Millennium priors prevent a confident assessment of the true ENSO response. Our results narrow the uncertainty of the mean equatorial Pacific conditions in the decades following the Mystery and Tambora eruption; when excluding western Pacific archives, all proxy subregions, including the eastern Pacific, provide evidence for cool conditions in the Niño-3.4 region. While we have built the case that models (and observations) that only simulate traditional ENSO covariance patterns generate inaccurate reconstructions during periods of high volcanic activity, it is unclear whether models with a more positive correlation coefficient between the Niño-3.4 and SPCZ region are more realistic. The Niño-3.4–SPCZ correlation coefficient is determined by the model's unforced tropical climate dynamics, simulation of volcanic eruptions, and partially by the initial conditions prior to the eruption. Ultimately, accurate paleo-DA reconstructions require simulations that capture the covariance patterns associated with boundary conditions not observed over the instrumental era. From our results, it is still not clear that the large tropical eruptions of the early nineteenth century instigated an El Niño–like response in the year following the eruption. Reconstructions seeking to reconstruct large, successive volcanic eruptions, as in the early nineteenth century, may require large multimodel ensembles of volcanically forced simulations. Additionally, volcanically forced slab ocean experiments could prove useful in differentiating the volcanically forced ENSO response from ENSO variability, as we have shown here.

4. Conclusions

Coral-based data assimilation has the potential to create skillful, high-resolution reconstructions of the tropical oceans. In this work, we combine a network of 125 coral archives with 10 climate model priors from the CMIP5/PMIP3 Past1000 experiments and 5 climate model priors from the CESM Last Millennium Ensemble to examine the behavior of tropical Pacific climate variability, with an emphasis on the Niño-3.4 region. We find that coral-only DA is more skillful in reconstructing the Niño-3.4 index than all-proxy DA during the instrumental era, particularly over the twentieth century. However, we find complications when extending this methodology into the early nineteenth century when the climate was strongly forced by two major volcanic eruptions.

TABLE 3. Super priors and relevant metrics detailing the behavior of the Niño-3.4 and SPCZ regions in the prior, as in Table 2.

Super prior	Description	Standard deviation of Niño-3.4 (°C)	Standard deviation of SPCZ region (°C)	Pearson's correlation coefficent (R) of Niño-3.4 and SPCZ
Super volcano	The prior was built using years 1800–50 from the CESM All Forcing and Volcanic Forcing simulations (consists of 18 50-yr segments, or 900 years) to encompass the large Mystery and Tambora eruptions.	0.93	0.31	−0.62
El Nada 0.05°C	The prior was built by identifying years of minimal Niño-3.4 variability in the CESM All Forcing simulations. We repeated this experiment several times, controlling the amount of variance allowed in the Niño-3.4 region. We ultimately conducted four experiments limiting the Niño-3.4 standard deviation to 0.05°C.	0.03	0.16	−0.13
EI Nada 0.15°C	As for El Nada 0.05°C, but Niño-3.4 standard deviation limited 0.15°C	0.09	0.19	−0.11
EI Nada 0.25°C	As for El Nada 0.05°C, but Niño-3.4 standard deviation limited 0.25°C	0.14	0.18	0.21
EI Nada 0.35°C	As for El Nada 0.05°C, but Niño-3.4 standard deviation limited 0.35°C	0.27	0.19	−0.30
Slab ocean	The prior CESM Large Ensemble slab ocean simulation provides a full atmospheric model that coupled to a single layer ''slab'' ocean, instead of a fully dynamical ocean. The oceanic component is simplified, is only thermodynamically coupled to the atmosphere.	0.18	0.21	−0.17

Reconstructions of Niño-3.4 temperatures are surprisingly diverse for decades after the 1809 Mystery and 1815 Tambora eruptions; the diversity is chiefly dependent on the assimilation of corals or continental proxies. We investigated the source of this persistent interproxy discrepancy by examining the influence of the PSMs, coral proxy records, and the fixed model priors on the reconstructed Niño-3.4 temperature. While the coral $\delta^{18}O$ bivariate PSM is more physically realistic, it amplifies the incorrect covariance relationship from the SPCZ region to the equatorial Pacific. The choice of a simplified linear PSM for coral $\delta^{18}O$ is ultimately not a major factor in the interproxy discrepancy. We find that many model priors capable of skillfully reconstructing the twentieth century generate unrealistic reconstructions during this interval due to the covariance relationships in their surface temperature fields in the equatorial Pacific. Covariance patterns associated with ENSO dominate the post-eruption response and can generate reconstructions at odds with results for proxies assimilated in isolation, nearly all of which indicate cold conditions. In many of the models considered in this study, the high anticorrelation of the Niño-3.4 and SPCZ regions causes the observations of persistent cool anomalies in the SPCZ to provoke unrealistic, decades long warm anomalies in reconstructions of the equatorial Pacific. This problem is not generic to all volcanic eruptions; both the early-nineteenth-century proxy network distribution and the exceptionally high-magnitude and successive nature of the Mystery and Tambora eruptions likely amplify the biased response. Later volcanic eruptions such as Krakatoa (1883) and Pinatubo (1991) lack these characteristics and do not feature similar interproxy discrepancies in the reconstructions.

This work emphasizes key differences in the magnitude and persistence of the post-eruption response within proxy archives and model simulations. We show that post-eruption covariance patterns appear to be quite different from that of unforced climate variability, even within the tropical Pacific. As such, we advise caution when using modern teleconnection patterns to interpret climate fields from proxies until covariance pattern sensitivity has been thoroughly investigated. The fact that assimilating individual records consistently reconstructs local cooling suggest that pan-Pacific cooling after large volcanic eruptions is a real feature of the climate system, although apparently few models can simulate such a response. Many of the models used in this study simulate a strong El Niño–like response in the annual mean following large eruptions, but our results indicate that may not be realistic. In simulations from the Past1000/Last Millennium experiments, large volcanic

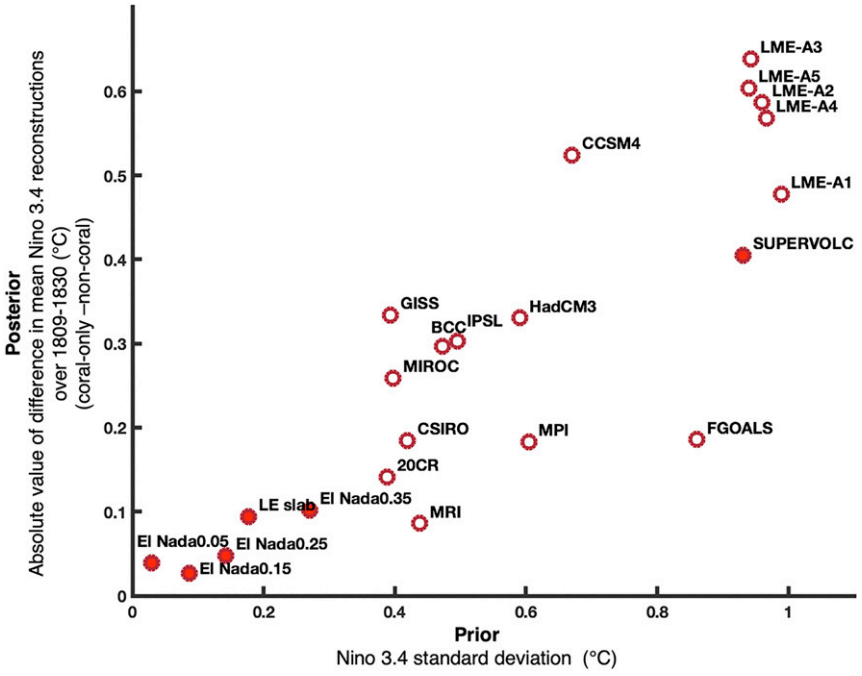

FIG. 8. Scatterplot of the relationship between the standard deviation of the Niño-3.4 in the prior and absolute value of the magnitude of the reconstructed interproxy discrepancy. Priors are sourced from the PMIP3/CMIP5 priors (unfilled circles) and super prior (filled circles) experiments.

eruptions provoke a short-term (on the order of a single year) but high-magnitude surface temperature response in the SPCZ region. However, proxy records suggest that volcanic eruptions provoke a multidecadal yet lower-magnitude surface temperature response in the SPCZ region. This observed cooling of the SPCZ region can force the reconstruction to have an unrealistically persistent, warm Niño-3.4 anomalies due to the SPCZ–Niño-3.4 teleconnection in the prior. Further investigation is required to evaluate if individual regions, such as the SPCZ region, are more susceptible to persistent anomalies following a volcanic eruption. If so, studies examining the dynamical mechanisms behind such persistence would be beneficial. Moreover, many of the coral records from the tropical Pacific do not span the years 1800–30, so additional coral records covering this interval would be valuable.

This work illustrates both the power and a critical weakness of paleoclimate data assimilation. It emphasizes the potential of the paleoclimate data assimilation methodology to examine the realism and robustness of proxy interpretations. These results narrow the uncertainty of the tropical climate response to the Mystery and Tambora volcanic eruptions of the early nineteenth century, suggesting cooler conditions across the tropical Pacific in the decades following the eruptions. However, this work also illustrates the problems that can arise when the climate model prior is strongly biased (such as the Pacific cold tongue bias) or not relevant to outlier events. Future work using paleo-DA to examine the ENSO response large volcanic eruptions could be enhanced first with more proxy observations from the central and eastern equatorial Pacific, and second through the use of highly diverse simulations of volcanic eruptions as a prior.

Acknowledgments. We thank Robert Tardif, Andre Perkins, and Luke Parsons for their efforts in troubleshooting bugs in code with S.C.S. S.C.S. was supported by the Joint Institute for the Study of the Atmosphere and Ocean's Postdoctoral Fellowship. We acknowledge support from NSF AGS-1702423 and NOAA NA18OAR4310422 to G.J.H. and support from NSF OCE-1536418 to C.P.S. We also thank Sylvia Dee and the two anonymous reviewers whose helpful comments clarified the manuscript.

Data availability statement. All model output used in this work can be found at the Earth System Grid Federation for the (past1000 experiments; https://esgf-node.llnl.gov/search/cmip5/) and the NCAR Earth System grid gateway (CESM experiments; https://www.earthsystemgrid.org/). All proxy data can be found on NOAA paleoclimate (https://www.ncdc.noaa.gov/data-access/paleoclimatology-data). Code to download and run Last Millennium reanalysis experiments can be found on the project documentation page (https://atmos.washington.edu/~hakim/lmr/docs/).

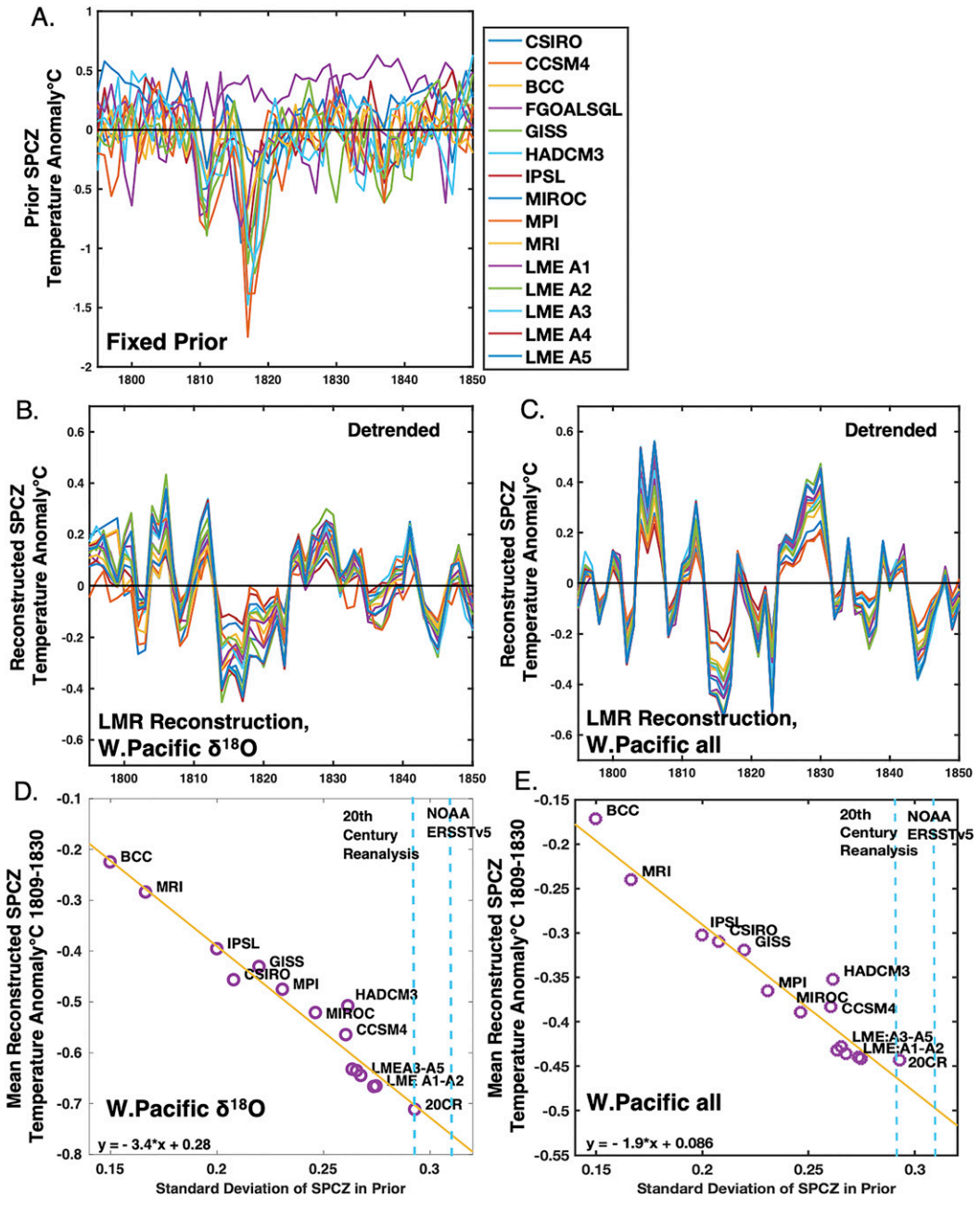

FIG. 9. Consistency in reconstructions of SPCZ temperature behavior. (a) Time series of the surface temperature anomalies in the prior over the SPCZ region. (b) Time series of reconstructed temperature anomalies in the SPCZ region (15°–25°S, 160°–210°E) assimilating only δ^{18}O records from the western Pacific. Reconstructions have been detrended with a fourth-degree polynomial over the years from 1780 to 2015. The years 1809–30 are anomalously cold. (c) As in (b), but reconstructions use all records from the western Pacific. (d) Scatterplot of the standard deviation of the SPCZ temperature in the fixed prior with the LMR reconstructed SPCZ temperature anomaly over the 1809–30 period assimilating only δ^{18}O records from the western Pacific. (e) As in (d), but SPCZ temperature reconstructions were determined by assimilating all western Pacific coral archives. All priors [except for FGOALS, which is excluded from (e) and (d)] illustrate a tight relationship between the variance in the prior and the magnitude of the anomaly in the reconstruction. Interestingly, reanalysis products show much more variance in the SPCZ region than any of the CMIP5 models, indicated by the dashed turquoise lines. (0.29°–0.31°C, 20CR and NOAA ERSSTv5, respectively).

REFERENCES

Adams, J. B., M. E. Mann, and C. M. Ammann, 2003: Proxy evidence for an El Niño–like response to volcanic forcing. *Nature*, **426**, 274–278, https://doi.org/10.1038/nature02101.

Alibert, C., and L. Kinsley, 2008: A 170-year Sr/Ca and Ba/Ca coral record from the western Pacific warm pool: 2. A window into variability of the New Ireland Coastal Undercurrent. *J. Geophys. Res.*, **113**, C06006, https://doi.org/10.1029/2007JC004263.

Asami, R., T. Yamada, Y. Iryu, T. M. Quinn, C. P. Meyer, and G. Paulay, 2005: Interannual and decadal variability of the western Pacific sea surface condition for the years 1787–2000: Reconstruction based on stable isotope record from a Guam coral. *J. Geophys. Res.*, **110**, C05018, https://doi.org/10.1029/2004JC002555.

Bagnato, S., B. K. Linsley, S. S. Howe, G. M. Wellington, and J. Salinger, 2005: Coral oxygen isotope records of interdecadal climate variations in the South Pacific Convergence Zone region. *Geochem. Geophys. Geosyst.*, **6**, Q06001, https://doi.org/10.1029/2004GC000879.

Batehup, R., S. McGregor, and A. J. E. Gallant, 2015: The influence of non-stationary teleconnections on palaeoclimate reconstructions of ENSO variance using a pseudoproxy framework. *Climate Past*, **11**, 1733–1749, https://doi.org/10.5194/cp-11-1733-2015.

Beck, J. W., R. L. Edwards, E. Ito, F. W. Taylor, J. Recy, F. Rougerie, P. Joannot, and C. Henin, 1992: Sea-surface temperature from coral skeletal strontium/calcium ratios. *Science*, **257**, 644–647, https://doi.org/10.1126/science.257.5070.644.

Bellenger, H., É. Guilyardi, J. Leloup, M. Lengaigne, and J. Vialard, 2014: ENSO representation in climate models: From CMIP3 to CMIP5. *Climate Dyn.*, **42**, 1999–2018, https://doi.org/10.1007/s00382-013-1783-z.

Brönnimann, S., and Coauthors, 2019: Last phase of the Little Ice Age forced by volcanic eruptions. *Nat. Geosci.*, **12**, 650–656, https://doi.org/10.1038/s41561-019-0402-y.

Brown, J. R., S. B. Power, F. P. Delage, R. A. Colman, A. F. Moise, and B. F. Murphy, 2011: Evaluation of the South Pacific convergence zone in IPCC AR4 climate model simulations of the twentieth century. *J. Climate*, **24**, 1565–1582, https://doi.org/10.1175/2010JCLI3942.1.

Charles, C. D., K. Cobb, M. D. Moore, and R. G. Fairbanks, 2003: Monsoon–tropical ocean interaction in a network of coral records spanning the 20th century. *Mar. Geol.*, **201**, 207–222, https://doi.org/10.1016/S0025-3227(03)00217-2.

Coats, S., J. E. Smerdon, B. I. Cook, and R. Seager, 2013: Stationarity of the tropical Pacific teleconnection to North America in CMIP5/PMIP3 model simulations. *Geophys. Res. Lett.*, **40**, 4927–4932, https://doi.org/10.1002/grl.50938.

Cole, J. E., and R. G. Fairbanks, 1990: The Southern Oscillation recorded in the δ18O of corals from Tarawa Atoll. *Paleoceanography*, **5**, 669–683, https://doi.org/10.1029/PA005i005p00669.

——, and E. R. Cook, 1998: The changing relationship between ENSO variability and moisture balance in the continental United States. *Geophys. Res. Lett.*, **25**, 4529–4532, https://doi.org/10.1029/1998GL900145.

——, R. B. Dunbar, T. R. McClanahan, and N. A. Muthiga, 2000: Tropical Pacific forcing of decadal SST variability in the western Indian Ocean over the past two centuries. *Science*, **287**, 617–619, https://doi.org/10.1126/science.287.5453.617.

Compo, G. P., and Coauthors, 2011: The Twentieth Century Reanalysis Project. *Quart. J. Roy. Meteor. Soc.*, **137**, 1–28, https://doi.org/10.1002/qj.776.

Conroy, J. L., K. M. Cobb, J. Lynch-Stieglitz, and P. J. Polissar, 2014: Constraints on the salinity–oxygen isotope relationship in the central tropical Pacific Ocean. *Mar. Chem.*, **161**, 26–33, https://doi.org/10.1016/j.marchem.2014.02.001.

——, D. M. Thompson, K. M. Cobb, D. Noone, S. Rea, and A. N. Legrande, 2017: Spatiotemporal variability in the δ18O–salinity relationship of seawater across the tropical Pacific Ocean. *Paleoceanography*, **32**, 484–497, https://doi.org/10.1002/2016PA003073.

Crowley, T. J., S. P. Obrochta, and J. Liu, 2014: Recent global temperature ''plateau'' in the context of a new proxy reconstruction. *Earth's Future*, **2**, 281–294, https://doi.org/10.1002/2013EF000216.

de Boisséson, E., M. A. Balmaseda, and M. Mayer, 2018: Ocean heat content variability in an ensemble of twentieth century ocean reanalyses. *Climate Dyn.*, **50**, 3783–3798, https://doi.org/10.1007/s00382-017-3845-0.

Dee, S., J. Emile-Geay, M. N. Evans, A. Allam, E. J. Steig, and D. M. Thompson, 2015: PRYSM: An open-source framework for PRoxY System Modeling, with applications to oxygen-isotope systems. *J. Adv. Model. Earth Syst.*, **7**, 1220–1247, https://doi.org/10.1002/2015MS000447.

——, Y. Okumura, S. Stevenson, and P. DiNezio, 2020a: Enhanced North American ENSO teleconnections during the Little Ice Age revealed by paleoclimate data assimilation. *Geophys. Res. Lett.*, **47**, e2020GL087504, https://doi.org/10.1029/2020GL087504.

——, K. M. Cobb, J. Emile-Geay, T. R. Ault, R. L. Edwards, H. Cheng, and C. D. Charles, 2020b: No consistent ENSO response to volcanic forcing over the last millennium. *Science*, **367**, 1477–1481, https://doi.org/10.1126/science.aax2000.

DeLong, K. L., T. M. Quinn, F. W. Taylor, K. Lin, and C.-C. Shen, 2012: Sea surface temperature variability in the southwest tropical Pacific since AD 1649. *Nat. Climate Change*, **2**, 799–804, https://doi.org/10.1038/nclimate1583.

——, J. A. Flannery, R. Z. Poore, T. M. Quinn, C. R. Maupin, K. Lin, and C.-C. Shen, 2014: A reconstruction of sea surface temperature variability in the southeastern Gulf of Mexico from 1734 to 2008 CE using cross-dated Sr/Ca records from the coral *Siderastrea siderea*. *Paleoceanography*, **29**, 403–422, https://doi.org/10.1002/2013PA002524.

Deser, C., and Coauthors, 2012: ENSO and Pacific decadal variability in the Community Climate System Model version 4. *J. Climate*, **25**, 2622–2651, https://doi.org/10.1175/JCLI-D-11-00301.1.

Ding, Y., J. A. Carton, G. A. Chepurin, G. Stenchikov, A. Robock, L. T. Sentman, and J. P. Krasting, 2014: Ocean response to volcanic eruptions in Coupled Model Intercomparison Project 5 simulations. *J. Geophys. Res. Oceans*, **119**, 5622–5637, https://doi.org/10.1002/2013JC009780.

Druffel, E. R. M., and S. Griffin, 1999: Variability of surface ocean radiocarbon and stable isotopes in the southwestern Pacific. *J. Geophys. Res.*, **104**, 232607–232613, https://doi.org/10.1029/1999JC900212.

——, ——, D. Vetter, R. B. Dunbar, and D. M. Mucciarone, 2015: Identification of frequent La Niña events during the early 1800s in the east equatorial Pacific. *Geophys. Res. Lett.*, **42**, 1512–1519, https://doi.org/10.1002/2014GL062997.

Dunbar, R. B., G. M. Wellington, M. W. Colgan, and P. W. Glynn, 1994: Eastern Pacific sea surface temperature since 1600 A.D.: The δ18O record of climate variability in Galápagos corals. *Paleoceanography*, **9**, 291–315, https://doi.org/10.1029/93PA03501.

Emile-Geay, J., R. Seager, M. A. Cane, E. R. Cook, and G. H. Haug, 2008: Volcanoes and ENSO over the past millennium. *J. Climate*, **21**, 3134–3148, https://doi.org/10.1175/2007JCLI1884.1.

——, and Coauthors, 2017: A global multiproxy database for temperature reconstructions of the Common Era. *Sci. Data*, **4**, 170088, https://doi.org/10.1038/sdata.2017.88.

Epstein, S., R. Buchsbaum, H. A. Lowenstam, and H. C. Urey, 1953: Revised carbonate-water isotopic temperature scale. *Geol. Soc. Amer. Bull.*, **64**, 1315–1326, https://doi.org/10.1130/0016-7606(1953)64[1315:RCITS]2.0.CO;2.

Evans, M. N., S. E. Tolwinski-Ward, D. M. Thompson, and K. J. Anchukaitis, 2013: Applications of proxy system modeling in high resolution paleoclimatology. *Quat. Sci. Rev.*, **76**, 16–28, https://doi.org/10.1016/j.quascirev.2013.05.024.

Fairbanks, R. G., M. N. Evans, J. L. Rubenstone, R. A. Mortlock, K. Broad, M. D. Moore, and C. D. Charles, 1997: Evaluating climate indices and their geochemical proxies measured in corals. *Coral Reefs*, **16**, S93–S100, https://doi.org/10.1007/s003380050245.

Felis, T., J. Pätzold, Y. Loya, M. Fine, A. H. Nawar, and G. Wefer, 2000: A coral oxygen isotope record from the northern Red Sea documenting NAO, ENSO, and North Pacific teleconnections on Middle East climate variability since the year 1750. *Paleoceanography*, **15**, 679–694, https://doi.org/10.1029/1999PA000477.

Gao, C., A. Robock, and C. Ammann, 2008: Volcanic forcing of climate over the past 1500 years: An improved ice core-based index for climate models. *J. Geophys. Res.*, **113**, D23111, https://doi.org/10.1029/2008JD010239.

Giese, B. S., and S. Ray, 2011: El Niño variability in simple ocean data assimilation (SODA), 1871–2008. *J. Geophys. Res.*, **116**, C02024, https://doi.org/10.1029/2010JC006695.

Goodkin, N. F., K. A. Hughen, S. C. Doney, and W. B. Curry, 2008: Increased multidecadal variability of the North Atlantic Oscillation since 1781. *Nat. Geosci.*, **1**, 844–848, https://doi.org/10.1038/ngeo352.

Gupta, M., and J. Marshall, 2018: The climate response to multiple volcanic eruptions mediated by ocean heat uptake: Damping processes and accumulation potential. *J. Climate*, **31**, 8669–8687, https://doi.org/10.1175/JCLI-D-17-0703.1.

Hakim, G. J., J. Emile-Geay, E. J. Steig, D. Noone, D. M. Anderson, R. Tardif, N. Steiger, and W. A. Perkins, 2016: The last millennium climate reanalysis project: Framework and first results. *J. Geophys. Res. Atmos.*, **121**, 6745–6764, https://doi.org/10.1002/2016JD024751.

Hansen, J., R. Ruedy, M. Sato, and K. Lo, 2010: Global surface temperature change. *Rev. Geophys.*, **48**, RG4004, https://doi.org/10.1029/2010RG000345.

Heiss, G. A., W.-C. Dullo, M. M. Joachimski, J. J. G. Reijmer, and H. Schuhmacher, 1999: Increased seasonality in the Gulf of Aqaba, Red Sea, recorded in the oxygen isotope record of a *Porites lutea* coral. *Senckenb. Marit.*, **30**, 17–26, https://doi.org/10.1007/BF03042826.

Hennekam, R., J. Zinke, E. van Sebille, M. ten Have, G.-J. A. Brummer, and G.-J. Reichart, 2018: Cocos (Keeling) corals reveal 200 years of multidecadal modulation of southeast Indian Ocean hydrology by Indonesian throughflow. *Paleoceanogr. Paleoclimatol.*, **33**, 48–60, https://doi.org/10.1002/2017PA003181.

Hirahara, S., M. Ishii, and Y. Fukuda, 2014: Centennial-scale sea surface temperature analysis and its uncertainty. *J. Climate*, **27**, 57–75, https://doi.org/10.1175/JCLI-D-12-00837.1.

Huang, B., and Coauthors, 2017: Extended reconstructed sea surface temperature, version 5 (ERSSTv5): Upgrades, validations, and intercomparisons. *J. Climate*, **30**, 8179–8205, https://doi.org/10.1175/JCLI-D-16-0836.1.

Hurrell, J. W., and Coauthors, 2013: The Community Earth System Model: A framework for collaborative research. *Bull. Amer. Meteor. Soc.*, **94**, 1339–1360, https://doi.org/10.1175/BAMS-D-12-00121.1.

Irving, D. B., and Coauthors, 2011: Evaluating global climate models for the Pacific island region. *Climate Res.*, **49**, 169–187, https://doi.org/10.3354/cr01028.

Kalnay, E., 2003: *Atmospheric Modeling, Data Assimilation and Predictability*. Cambridge University Press, 341 pp.

Kaplan, A., Y. Kushnir, M. A. Cane, and M. B. Blumenthal, 1997: Reduced space optimal analysis for historical data sets: 136 years of Atlantic sea surface temperatures. *J. Geophys. Res.*, **102**, 272835–272860, https://doi.org/10.1029/97JC01734.

Kay, J. E., and Coauthors, 2015: The Community Earth System Model (CESM) large ensemble project: A community resource for studying climate change in the presence of internal climate variability. *Bull. Amer. Meteor. Soc.*, **96**, 1333–1349, https://doi.org/10.1175/BAMS-D-13-00255.1.

Khodri, M., and Coauthors, 2017: Tropical explosive volcanic eruptions can trigger El Niño by cooling tropical Africa. *Nat. Commun.*, **8**, 778, https://doi.org/10.1038/s41467-017-00755-6.

Kilbourne, K. H., T. M. Quinn, R. Webb, T. Guilderson, J. Nyberg, and A. Winter, 2008: Paleoclimate proxy perspective on Caribbean climate since the year 1751: Evidence of cooler temperatures and multidecadal variability. *Paleoceanography*, **23**, PA3220, https://doi.org/10.1029/2008PA001598.

Kim, S.-T., and J. R. O'Neil, 1997: Equilibrium and nonequilibrium oxygen isotope effects in synthetic carbonates. *Geochim. Cosmochim. Acta*, **61**, 3461–3475, https://doi.org/10.1016/S0016-7037(97)00169-5.

Kuhnert, H., J. Pätzold, B. Hatcher, K.-H. Wyrwoll, A. Eisenhauer, L. B. Collins, Z. R. Zhu, and G. Wefer, 1999: A 200-year coral stable oxygen isotope record from a high-latitude reef off Western Australia. *Coral Reefs*, **18**, 1–12, https://doi.org/10.1007/s003380050147.

——, T. Crüger, and J. Pätzold, 2005: NAO signature in a Bermuda coral Sr/Ca record. *Geochem. Geophys. Geosyst.*, **6**, Q04004, https://doi.org/10.1029/2004GC000786.

Lawman, A. E., J. W. Partin, S. G. Dee, C. A. Casadio, P. DiNezio, and T. M. Quinn, 2020: Developing a coral proxy system model to compare coral and climate model estimates of changes in Paleo-ENSO variability. *Paleoceanogr. Paleoclimatol.*, **35**, e2019PA003836, https://doi.org/10.1029/2019PA003836.

LeGrande, A. N., and G. A. Schmidt, 2006: Global gridded data set of the oxygen isotopic composition in seawater. *Geophys. Res. Lett.*, **33**, L12604, https://doi.org/10.1029/2006GL026011.

Lehner, F., A. P. Schurer, G. C. Hegerl, C. Deser, and T. L. Frölicher, 2016: The importance of ENSO phase during volcanic eruptions for detection and attribution. *Geophys. Res. Lett.*, **43**, 2851–2858, https://doi.org/10.1002/2016GL067935.

Li, G., and S.-P. Xie, 2014: Tropical biases in CMIP5 multimodel ensemble: The excessive equatorial Pacific cold tongue and double ITCZ problems. *J. Climate*, **27**, 1765–1780, https://doi.org/10.1175/JCLI-D-13-00337.1.

Lin, J.-L., 2007: The double-ITCZ problem in IPCC AR4 coupled GCMs: Ocean–atmosphere feedback analysis. *J. Climate*, **20**, 4497–4525, https://doi.org/10.1175/JCLI4272.1.

Linsley, B. K., R. B. Dunbar, G. M. Wellington, and D. A. Mucciarone, 1994: A coral-based reconstruction of intertropical convergence zone variability over Central America since 1707. *J. Geophys. Res.*, **99**, 9977–9994, https://doi.org/10.1029/94JC00360.

——, A. Kaplan, Y. Gouriou, J. Salinger, P. B. Demenocal, G. M. Wellington, and S. S. Howe, 2006: Tracking the extent of the South Pacific convergence zone since the early 1600s. *Geochem. Geophys. Geosyst.*, **7**, Q05003, https://doi.org/10.1029/2005GC001115.

Lough, J. M., 2004: A strategy to improve the contribution of coral data to high-resolution paleoclimatology. *Palaeogeogr. Palaeoclimatol. Palaeoecol.*, **204**, 115–143, https://doi.org/10.1016/S0031-0182(03)00727-2.

Maher, N., S. McGregor, M. H. England, and A. Sen Gupta, 2015: Effects of volcanism on tropical variability. *Geophys. Res. Lett.*, **42**, 6024–6033, https://doi.org/10.1002/2015GL064751.

Mann, M. E., M. A. Cane, S. E. Zebiak, and A. Clement, 2005: Volcanic and solar forcing of the tropical Pacific over the past 1000 years. *J. Climate*, **18**, 447–456, https://doi.org/10.1175/JCLI-3276.1.

McGregor, S., and A. Timmermann, 2011: The effect of explosive tropical volcanism on ENSO. *J. Climate*, **24**, 2178–2191, https://doi.org/10.1175/2010JCLI3990.1.

Murty, S. A., N. F. Goodkin, A. A. Wiguna, and A. L. Gordon, 2018: Variability in coral-reconstructed sea surface salinity between the northern and southern Lombok Strait linked to East Asian winter monsoon mean state reversals. *Paleoceanogr. Paleoclimatol.*, **33**, 1116–1133, https://doi.org/10.1029/2018PA003387.

Nash, J., and J. Sutcliffe, 1970: River flow forecasting through conceptual models: Part I—A discussion of principles. *J. Hydrol.*, **10**, 282–290, https://doi.org/10.1016/0022-1694(70)90255-6.

Newhall, C. G., and S. Self, 1982: The volcanic explosivity index (VEI): An estimate of explosive magnitude for historical volcanism. *J. Geophys. Res.*, **87**, 1231–1238, https://doi.org/10.1029/JC087iC02p01231.

Ohba, M., H. Shiogama, T. Yokohata, and M. Watanabe, 2013: Impact of strong tropical volcanic eruptions on ENSO simulated in a coupled GCM. *J. Climate*, **26**, 5169–5182, https://doi.org/10.1175/JCLI-D-12-00471.1.

O'Neil, J. R., R. N. Clayton, and T. K. Mayeda, 1969: Oxygen isotope fractionation in divalent metal carbonates. *J. Chem. Phys.*, **51**, 5547–5558, https://doi.org/10.1063/1.1671982.

Osborne, M. C., R. B. Dunbar, D. A. Mucciarone, E. Druffel, and J.-A. Sanchez-Cabeza, 2014: A 215-yr coral δ^{18}O time series from Palau records dynamics of the West Pacific warm pool following the end of the Little Ice Age. *Coral Reefs*, **33**, 719–731, https://doi.org/10.1007/s00338-014-1146-1.

Otto-Bliesner, B., 2014: CCSM4 coupled simulation for CMIP5 past 1000 years (850–1850) with natural forcings, served by ESGF. World Data Center for Climate (WDCC) at DKRZ, accessed October 2018, https://doi.org/10.1594/WDCC/CMIP5.NRS4pk.

——, and Coauthors, 2016: Climate variability and change since 850 CE: An ensemble approach with the Community Earth System Model. *Bull. Amer. Meteor. Soc.*, **97**, 735–754, https://doi.org/10.1175/BAMS-D-14-00233.1.

Pausata, F., L. Chafik, R. Caballero, and D. S. Battisti, 2015: Impacts of high-latitude volcanic eruptions on ENSO and AMOC. *Proc. Natl. Acad. Sci. USA*, **112**, 132784–132788, https://doi.org/10.1073/pnas.1509153112.

——, C. Karamperidou, R. Caballero, and D. S. Battisti, 2016: ENSO response to high-latitude volcanic eruptions in the Northern Hemisphere: The role of the initial conditions. *Geophys. Res. Lett.*, **43**, 8694–8702, https://doi.org/10.1002/2016GL069575.

Predybaylo, E., G. L. Stenchikov, A. T. Wittenberg, and F. Zeng, 2017: Impacts of a Pinatubo-size volcanic eruption on ENSO. *J. Geophys. Res. Atmos.*, **122**, 925–947, https://doi.org/10.1002/2016JD025796.

Quinn, T. M., T. J. Crowley, and F. W. Taylor, 1996: New stable isotope results from a 173-year coral from Espiritu Santo, Vanuatu. *Geophys. Res. Lett.*, **23**, 3413–3416, https://doi.org/10.1029/96GL03169.

——, ——, ——, C. Henin, P. Joannot, and Y. Join, 1998: A multicentury stable isotope record from a New Caledonia coral: Interannual and decadal sea surface temperature variability in the southwest Pacific since 1657 A.D. *Paleoceanography*, **13**, 412–426, https://doi.org/10.1029/98PA00401.

Rayner, N. A., D. E. Parker, E. B. Horton, C. K. Folland, L. V. Alexander, D. P. Rowell, E. C. Kent, and A. Kaplan, 2003: Global analyses of sea surface temperature, sea ice, and night marine air temperature since the late nineteenth century. *J. Geophys. Res.*, **108**, 4407, https://doi.org/10.1029/2002JD002670.

Roemmich, D., and J. Gilson, 2009: The 2004–2008 mean and annual cycle of temperature, salinity, and steric height in the global ocean from the Argo Program. *Prog. Oceanogr.*, **82**, 81–100, https://doi.org/10.1016/j.pocean.2009.03.004.

Russon, T., A. W. Tudhope, G. C. Hegerl, M. Collins, and J. Tindall, 2013: Inter-annual tropical Pacific climate variability in an isotope-enabled CGCM: Implications for interpreting coral stable oxygen isotope records of ENSO. *Climate Past*, **9**, 1543–1557, https://doi.org/10.5194/cp-9-1543-2013.

Samanta, D., K. B. Karnauskas, and N. F. Goodkin, 2019: Tropical Pacific SST and ITCZ biases in climate models: Double trouble for future rainfall projections? *Geophys. Res. Lett.*, **46**, 2242–2252, https://doi.org/10.1029/2018GL081363.

Sanchez, S. C., C. D. Charles, J. D. Carriquiry, and J. A. Villaescusa, 2016: Two centuries of coherent decadal climate variability across the Pacific North American region. *Geophys. Res. Lett.*, **43**, 9208–9216, https://doi.org/10.1002/2016GL069037.

Schmidt, G. A., and Coauthors, 2011: Climate forcing reconstructions for use in PMIP simulations of the last millennium (v1. 0). *Geosci. Model Dev.*, **4**, 33–45, https://doi.org/10.5194/gmd-4-33-2011.

Shi, L., and Coauthors, 2017: An assessment of upper ocean salinity content from the Ocean Reanalyses Intercomparison Project (ORA-IP). *Climate Dyn.*, **49**, 1009–1029, https://doi.org/10.1007/s00382-015-2868-7.

Singh, H. K. A., G. J. Hakim, R. Tardif, J. Emile-Geay, and D. C. Noone, 2018: Insights into Atlantic multidecadal variability using the Last Millennium Reanalysis framework. *Climate Past*, **14**, 157–174, https://doi.org/10.5194/cp-14-157-2018.

Steiger, N. J., G. J. Hakim, E. J. Steig, D. S. Battisti, and G. H. Roe, 2014: Assimilation of time-averaged pseudoproxies for climate reconstruction. *J. Climate*, **27**, 426–441, https://doi.org/10.1175/JCLI-D-12-00693.1.

——, J. E. Smerdon, E. R. Cook, and B. I. Cook, 2018: A reconstruction of global hydroclimate and dynamical variables over the Common Era. *Sci. Data*, **5**, 180086, https://doi.org/10.1038/sdata.2018.86.

Stevenson, S., B. S. Powell, M. A. Merrifield, K. M. Cobb, J. Nusbaumer, and D. Noone, 2015: Characterizing seawater oxygen isotopic variability in a regional ocean modeling framework: Implications for coral proxy records. *Paleoceanography*, **30**, 1573–1593, https://doi.org/10.1002/2015PA002824.

——, B. Otto-Bliesner, J. Fasullo, and E. Brady, 2016: "El Niño like" hydroclimate responses to last millennium volcanic eruptions. *J. Climate*, **29**, 2907–2921, https://doi.org/10.1175/JCLI-D-15-0239.1.

——, J. T. Fasullo, B. L. Otto-Bliesner, R. A. Tomas, and C. Gao, 2018: Role of eruption season in reconciling model and proxy responses to tropical volcanism. *Proc. Natl. Acad. Sci. USA*, **114**, 1822–1826, https://doi.org/10.1073/pnas.1612505114.

Stommel, H., and E. Stommel, 1979: The year without a summer. *Sci. Amer.*, **240**, 176–187, https://doi.org/10.1038/scientificamerican0679-176.

Stothers, R. B., 1984: The great Tambora eruption in 1815 and its aftermath. *Science*, **224**, 1191–1198, https://doi.org/10.1126/science.224.4654.1191.

Swart, P. K., R. E. Dodge, and H. J. Hudson, 1996a: A 240-year stable oxygen and carbon isotopic record in a coral from South Florida: Implications for the prediction of precipitation in southern Florida. *Palaios*, **11**, 362–375, https://doi.org/10.2307/3515246.

——, G. F. Healy, R. E. Dodge, P. Kramer, J. H. Hudson, R. B. Halley, and M. B. Robblee, 1996b: The stable oxygen and carbon isotopic record from a coral growing in Florida Bay: A 160 year record of climatic and anthropogenic influence. *Palaeogeogr. Palaeoclimatol. Palaeoecol.*, **123**, 219–237, https://doi.org/10.1016/0031-0182(95)00078-X.

Tangri, N., R. B. Dunbar, B. K. Linsley, and D. M. Mucciarone, 2018: ENSO's shrinking twentieth-century footprint revealed in a half-millennium coral core from the South Pacific Convergence Zone. *Paleoceanogr. Paleoclimatol.*, **33**, 1136–1150, https://doi.org/10.1029/2017PA003310.

Tardif, R., and Coauthors, 2019: Last Millennium Reanalysis with an expanded proxy database and seasonal proxy modeling. *Climate Past*, **15**, 1251–1273, https://doi.org/10.5194/cp-15-1251-2019.

Thompson, D. M., T. R. Ault, M. N. Evans, J. E. Cole, and J. Emile-Geay, 2011: Comparison of observed and simulated tropical climate trends using a forward model of coral δ^{18}O. *Geophys. Res. Lett.*, **38**, L14706, https://doi.org/10.1029/2011GL048224.

Tierney, J. E., and Coauthors, 2015: Tropical sea surface temperatures for the past four centuries reconstructed from coral archives. *Paleoceanography*, **30**, 226–252, https://doi.org/10.1002/2014PA002717.

Timmreck, C., S. J. Lorenz, T. J. Crowley, S. Kinne, T. J. Raddatz, M. A. Thomas, and J. H. Jungclaus, 2009: Limited temperature response to the very large AD 1258 volcanic eruption. *Geophys. Res. Lett.*, **36**, L21708, https://doi.org/10.1029/2009GL040083.

Weber, J. N., and P. M. J. Woodhead, 1972: Temperature dependence of oxygen-18 concentration in reef coral carbonates. *J. Geophys. Res.*, **77**, 463–473, https://doi.org/10.1029/JC077i003p00463.

Whitaker, J. S., and T. M. Hamill, 2002: Ensemble data assimilation without perturbed observations. *Mon. Wea. Rev.*, **130**, 1913–1924, https://doi.org/10.1175/1520-0493(2002)130<1913:EDAWPO>2.0.CO;2.

Wu, H. C., B. K. Linsley, E. P. Dassié, B. Schiraldi, and P. B. deMenocal, 2013: Oceanographic variability in the South Pacific Convergence Zone region over the last 210 years from multi-site coral Sr/Ca records. *Geochem. Geophys. Geosyst.*, **14**, 1435–1453, https://doi.org/10.1029/2012GC004293.

Zanchettin, D., C. Timmreck, H.-F. Graf, A. Rubino, S. Lorenz, K. Lohmann, K. Krüger, and J. H. Jungclaus, 2012: Bi-decadal variability excited in the coupled ocean–atmosphere system by strong tropical volcanic eruptions. *Climate Dyn.*, **39**, 419–444, https://doi.org/10.1007/s00382-011-1167-1.

——, and Coauthors, 2016: The Model Intercomparison Project on the Climatic Response to Volcanic Forcing (VolMIP): Experimental design and forcing input data for CMIP6. *Geosci. Model Dev.*, **9**, 2701–2719, https://doi.org/10.5194/gmd-9-2701-2016.

——, C. Timmreck, M. Toohey, J. H. Jungclaus, M. Bittner, S. J. Lorenz, and A. Rubino, 2019: Clarifying the relative role of forcing uncertainties and initial-condition unknowns in spreading the climate response to volcanic eruptions. *Geophys. Res. Lett.*, **46**, 1602–1611, https://doi.org/10.1029/2018GL081018.

Zinke, J., W.-C. Dullo, G. A. Heiss, and A. Eisenhauer, 2004: ENSO and Indian Ocean subtropical dipole variability is recorded in a coral record off southwest Madagascar for the period 1659 to 1995. *Earth Planet. Sci. Lett.*, **228**, 177–194, https://doi.org/10.1016/j.epsl.2004.09.028.

——, A. Rountrey, M. Feng, S.-P. Xie, D. Dissard, K. Rankenburg, J. M. Lough, and M. T. McCulloch, 2014: Corals record long-term Leeuwin Current variability including Ningaloo Niño/Niña since 1795. *Nat. Commun.*, **5**, 3607, https://doi.org/10.1038/ncomms4607.

——, and Coauthors, 2015: Coral record of southeast Indian Ocean marine heatwaves with intensified western Pacific temperature gradient. *Nat. Commun.*, **6**, 8562, https://doi.org/10.1038/ncomms9562.